Accepted Manuscript online: 2022-09-12 Article published online: 2022-10-26

An Azobenzene-Clamped Bichromophore

Nils Schmickler[a]
David A. Hofmeister[a]
Joshua Bahr[a]
Jakob Schedlbauer[b]
Stefan-S. Jester*[a]
John M. Lupton*[b]
Sigurd Höger*[a]

[a] Kekulé-Institut für Organische Chemie und Biochemie, Rheinische Friedrich-Wilhelms-Universität Bonn, Gerhard-Domagk-Str. 1, 53121 Bonn, Germany
[b] Institut für Experimentelle und Angewandte Physik, Universität Regensburg, Universitätsstr. 31, 93053 Regensburg, Germany
* stefan.jester@uni-bonn.de; john.lupton@physik.uni-regensburg.de; hoeger@uni-bonn.de

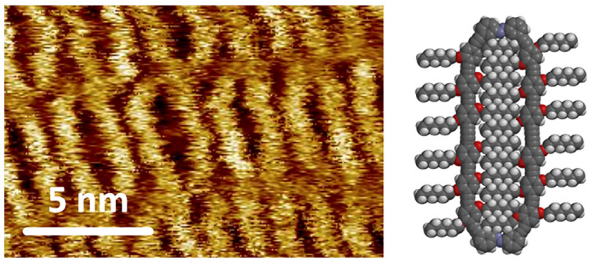

Received: 12.07.2022
Accepted after revision: 30.08.2022
DOI: 10.1055/a-1941-7757; Art ID: OM-2022-07-0021-OA

Abstract An azo-clamped nanoscale bichromophoric cyclophane is synthesized by the intramolecular Pd(II)-catalyzed coupling of the corresponding bisacetylenic precursor. The two azo moieties in the latter can adopt *cis* and *trans* configurations. Thin-layer chromatography shows only two spots, and by scanning tunneling microscopy the *trans*/*trans* and *cis*/*cis* isomers are found. The final cyclophane does not show any switching behavior at all, but dense and wide structures are visualized after adsorption to highly oriented pyrolytic graphite. Photophysical investigations of the cyclophane show that most of the fluorescence is quenched, most likely due to the azo clamp. However, bright molecules show nearly perfect single-photon emission, meaning that efficient energy transfer between the two chromophores takes place within the molecule.

Key words: cyclophanes, azo-switches, phenylene–ethynylene–butadiynylenes, scanning tunneling microscopy, single-molecule spectroscopy

Introduction

π-Conjugated materials, low-molecular-weight compounds as well as polymers have interesting optical and electronic properties, making them active components in organic electronics like organic light-emitting diodes, organic solar cells, and organic field-effect transistors. Further improvement of the devices requires a deeper understanding of the interaction of the molecular segments in the ground state and in the excited state, both within one and between two or more molecular species.[1–4] The latter is of outstanding importance since devices, even though generally containing the electroactive materials in form of a thin film, have thousands of billions of single molecules.

Modern synthetic methodologies as well as sophisticated spectroscopic techniques, also on the single-molecule level, are used to make a large variety of elaborated conjugated model compounds available now and allow studying their fundamental optical behavior in conjugated molecules.[5–8] Single-molecule fluorescence spectroscopy allows the investigation of individual molecules and gives detailed information on the fluorescence energy, the vibronic structure as well as life-time and polarization, information that is averaged when bulk measurements are performed. However, studying discrete aggregates, e.g. dimers or trimers of oligomers, rather seems like an oxymoron: to perform the single-molecule measurement, the analyte molecule is diluted in a solvent to single-molecule concentration (~10^{-12} M) and mixed with a polymethyl methacrylate (PMMA)/toluene solution. This solution is then dynamically spin-coated, resulting in a film thickness of roughly 100 nm, in which the separated single molecules can be investigated. It is clear that most molecules are isolated in the matrix, and even if a few dimers or larger aggregates might be observed, the units comprising these are randomly oriented with respect to each other. A way out of this dilemma is defined multichromophoric aggregates, where not only the number of individual chromophores but also their relative spacing and orientation can be specified. We recently described a number of clamped oligomers with various lengths and distances.[9–13] Specifically, we connected poly(phenylene–ethynylene–butadiynylene)s[14] with defined lengths between 5 and 10 nm at their ends, so that they are held at distances between 0.38 and 2.1 nm, forming shape-persistent macrocycles.[15] The distance is measured at the clamp positions and might differ in the molecule center due to a restricted persistence length of the phenylene–ethynylene–

butadiynylene rods.[16] One possibility to rigidify phenylene–ethynylene–butadiynylenes is ladderization.[17] We also synthesized and investigated in detail a trichromophoric oligomer system, in which the spatial separation between the clamped three oligomers is around 0.7 nm.[13] However, in all these cases the distances between the oligomers are, apart from thermal fluctuations, constant. Since the coupling between the oligomers is sensitive to their spacing, we describe here a bichromophore with azo clamps in the hope that a change of the coupling can be observed when a light-driven photoisomerization of the azo moieties of the macrocycle can be realized.[18] Azobenzenes, after their first description in the 1830 s[19] and the determination of their structure 30 years later,[20] have become an important class of industrial colorants and still represent more than half of the industrially produced dyes.[21] A hundred years after their first description, the light-induced isomerization of the azo moiety was reported.[22] This was the starting point for the implementation of azo moieties for light-induced structure and function alteration of linear and cyclic molecules of different sizes and functionalities.[23]

Results and Discussion

The straightforward synthesis of the azo-containing bichromophoric cyclophane **1** presented here is shown in Scheme 1. **1** is an azo-analogue of our recently described clamp structure, i.e. **2**.[12] 3,3-Diiodoazobenzene (**3**)[24] was coupled with the monoprotected bisacetylene **4**[25] to give **5** in a yield of about 71% after purification by column chromatography and recycling gel permeation chromatography (rec GPC). However, **5** contains small amounts of the Glaser side product that could not be removed at this stage of the reaction sequence. Nevertheless, after statistical deprotection of **5**, the mono-protected bisacetylene **6a** (32%) along with the completely deprotected byproduct **6b** (29%) were obtained in the pure form. Attempts to cyclodimerize **6b** to **1** using CuCl and $CuCl_2$ in pyridine were not successful and gave only the starting material, acyclic dimer, and unknown byproducts of higher molecular weight. The route of success was first a dimerization of the monoprotected "half-ring" **6a** to **7** (48%), deprotection of the acetylenes (81%), and intramolecular ring-closure to **1** (50–60%) using Pd(II) and Cu(I) as a catalyst system, I_2 as an oxidant and diisopropylamine as a base in THF. As expected, upon cyclization the hydrodynamic radius of the compound decreases dramatically, leading to a large change in the GPC-determined molecular weight (vs. polystyrene), although only two hydrogen atoms are removed (see the Supporting Information, SI).

While the NMR spectrum of the intermediates shows the presence of *cis* and *trans* azobenzene units, in the final macrocycle the azobenzene units cannot be switched to the *cis* isomers, most probably due to steric reasons of the transition state of the isomerization since space-filling models of *trans*/*trans*-**1** and *cis*/*cis*-**1** show no significant deformation of the chromophores. Thus, the proposed photoinduced alteration of the chromophore–chromophore distance is not realized in this compound **1**.

Although the absence of any switching behavior in a smaller macrocycle has been reported,[26] we expected that the large ring would give the system enough flexibility to allow for a photoinduced change of the azo conformation.[27] Speculations about the large π-system being responsible for the stabilization of the *trans*-conformation can be discarded, since **6b** and **8** undergo reversible *trans*–*cis* switching (vide infra).

Self-assembled monolayers of **1** and **8** at the solid/liquid interface of the respective compound in 1,2,4-trichlorobenzene (TCB) and highly oriented pyrolytic graphite (HOPG) were investigated by scanning tunneling microscopy (STM).

At a concentration of **1** of 5×10^{-6} M in the supernatant liquid phase, **1** forms (after thermal annealing for 20 s to 80 °C, a routine procedure for enhancing self-assembly and packing order) a densely covered self-assembled monolayer with domain sizes of similarly oriented molecules in the range of 20×20 nm^2 (see the overview STM image in the SI). In the high-resolution STM image shown in Figure 1a, each molecule of **1** is imaged as a pair of bright lines (attributed to the rigid rod units) connected by two medium-bright regions (attributed to the azobenzene units). The rigid rods neither appear as perfect lines, nor do they all have the same shape. More precisely, wide pairs of rods (as, e.g., those marked by arrow 1 in Figure 1a) should provide space for all (or most) of the alkoxy side chains being aligned along the HOPG surface, while tight pairs of rods (e.g., those marked by arrow 2 in Figure 1a) might correspond to alkoxy side chains pointing towards the solution phase (see SI). Their random occurrence correlates with some degree of disorder of the otherwise two-dimensionally (2D) crystalline domains, to which a unit cell of $a = (5.1 \pm 0.2)$ nm, $b = (3.1 \pm 0.2)$ nm, $\gamma\,(a, b) = (78 \pm 2)^\circ$ and an orthogonal orientation of the backbones, *c*, to one of the HOPG main axis directions, *d*, is indexed. An idealized supramolecular model (of a geometry-optimized wide conformer with all hexyloxy side chains adsorbed in parallel to the HOPG surface and along one of its main axis directions, see SI) is shown in Figure 1c.

At a concentration of **8** of 10^{-5} M in the supernatant liquid phase, **8** covers the surface densely (after thermal annealing for 20 s to 80 °C). An overview STM image (see SI) shows domains of parallel-aligned backbones, however with disorder. In the detailed STM image (Figure 1b), one dimensionally (1D) crystalline domains are observed, each consisting of a few molecules. The image region in Figure 1b marked by the white dots is translated to the supramolecular model in Figure 1d. In this region, five molecules of **8** are aligned in parallel, and a unit vector of $a = (1.4 \pm 0.1)$ nm is indexed. Their azobenzene units adopt the *trans*/*trans* configuration,

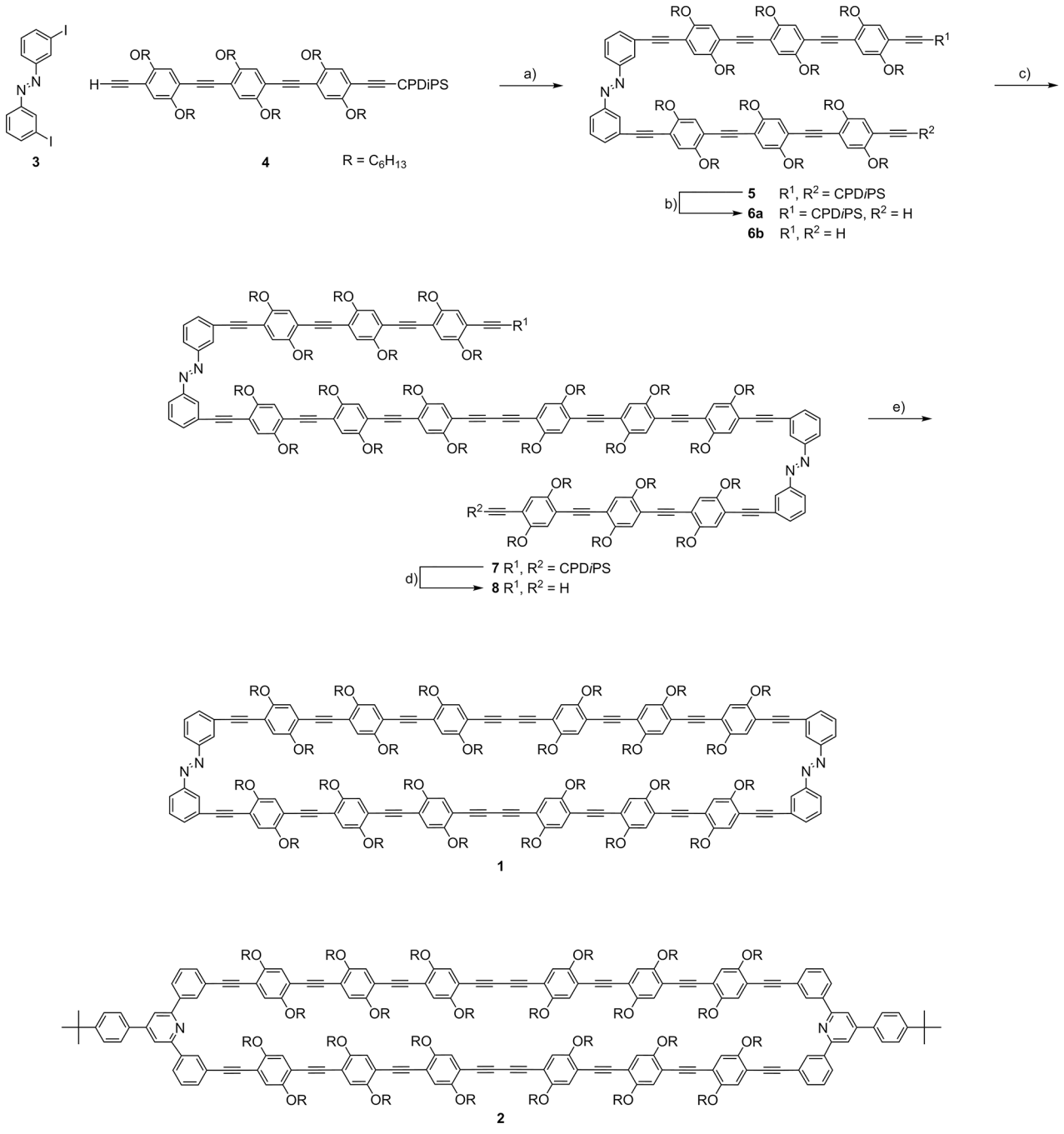

Scheme 1 a) $Pd(PPh_3)_4$, CuI, piperidine, THF, rt, 6 d, 71%; b) TBAF (1 M in THF), THF, H_2O (5 vol%), rt, 5 h, 32%; c) $Pd(PPh_3)_2Cl_2$, CuI, I_2, $HN(iPr)_2$, THF, rt, 16 h, 48%; d) TBAF (1 M in THF), THF, rt, 12 h, 81%; e) $Pd(PPh_3)_2Cl_2$, CuI, I_2, $HN(iPr)_2$, THF, 50–60%.

and are oriented *anti* relative to the central rigid rod. Moreover, the rigid rod units at each of the azobenzene units are oriented in the *anti*-conformation (cf. Figure S8). The distance of the molecules is defined by intermolecularly interdigitating hexyloxy side chains that are aligned along one of the HOPG main axis directions, *d*. The rigid rods are oriented along *c* with γ (*c*, *d*) = (83 ± 2)° relative to one of the HOPG main axis directions, *d*, and the unit cell vector, *a*, is oriented relative to *d* with γ (*a*, *d*) = (7 ± 2)°. In the marked surface region, two more molecules of **8** are shifted in parallel (along

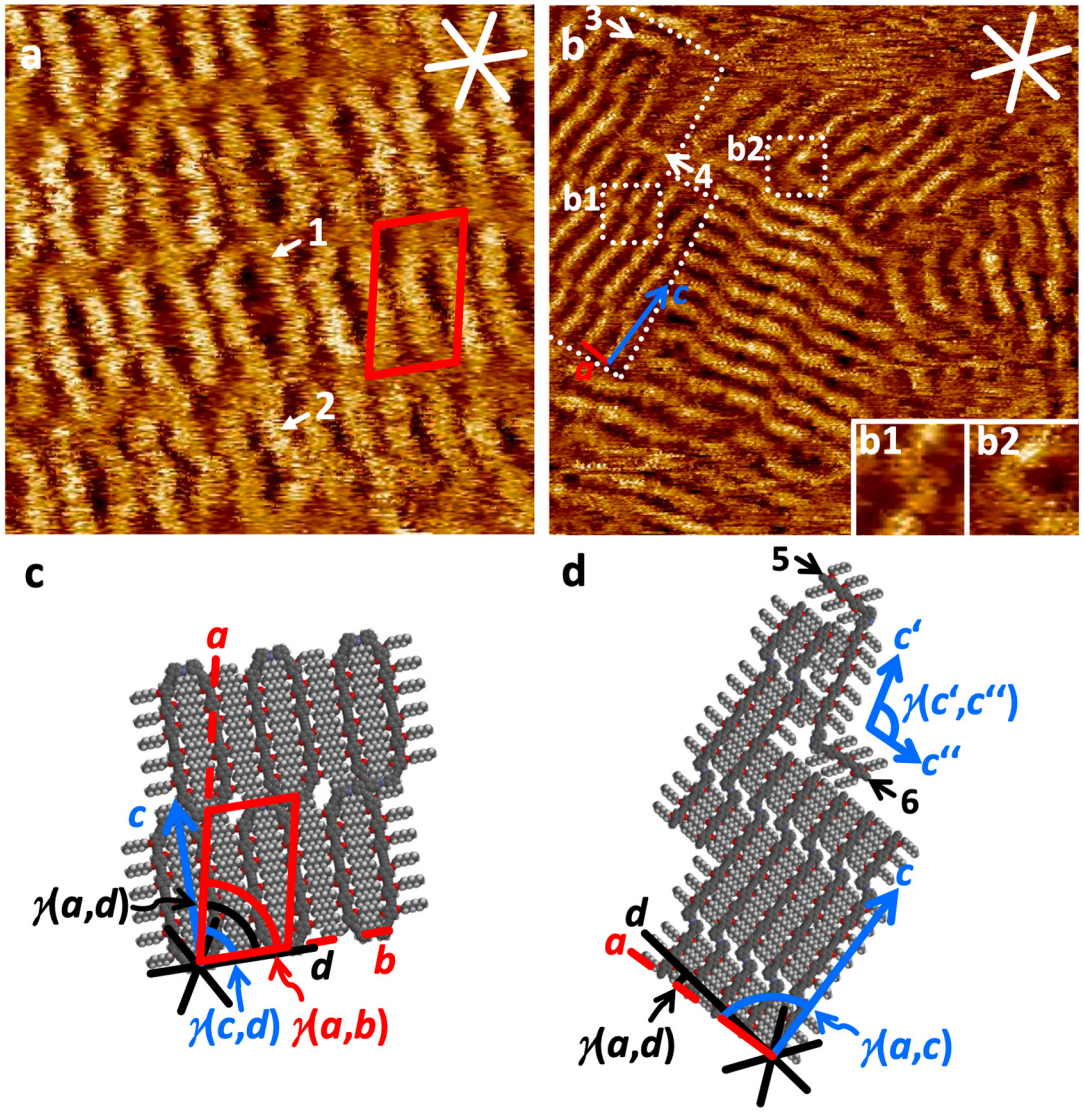

Figure 1 (a, b) Scanning tunneling microscopy images and (c, d) (supra-)molecular models of (a), (c) **1** and (b), (b1), (b2), (d) **8** at the solid/liquid interface of highly oriented pyrolytic graphite (HOPG) and solutions of the respective compounds in 1,2,4-trichlorobenzene. Image parameters: (a) 18×18 nm^2, $V_S = -0.8$ V, $I_t = 55$ pA, $c = 5 \times 10^{-6}$ M, sample thermally annealed for 20 s to 80 °C prior to imaging; unit cell $a = (5.1 \pm 0.2)$ nm, $b = (3.1 \pm 0.2)$ nm, γ (a, b) = $(78 \pm 2)°$; additional packing parameters: γ (c, d) = $(90 \pm 3)°$, $b \parallel d$; (b): 30×30 nm^2, $V_S = -1.1$ V, $I_t = 117$ pA; $c = 1 \times 10^{-5}$ M, sample thermally annealed for 20 s to 80 °C prior to imaging; unit cell $a = (1.4 \pm 0.1)$ nm; additional packing parameters: γ (c, d) = $(83 \pm 2)°$, γ (a, d) = $(7 \pm 2)°$; (b1), (b2): each 2.1×2.1 nm^2. Red and white (black) lines as well as blue arrows indicate unit cell vectors, HOPG main axis directions, and backbone directions, respectively.

c) by half a molecule length relative to the five previously discussed molecules, so that seven *trans*-azobenzene units (each with two rigid rods in the *anti*-conformation) form a row. Notably, **8** in the periodic packing adopts a linear shape with two kinks, attributed to the azobenzene units. One example of a *trans*-azobenzene unit is magnified in Figure 1b1 and is clearly distinguishable from the *cis*-azobenzene unit shown in Figure 1b2. Moreover (and despite the thermal annealing procedure), a single molecule of *cis*/*cis*-**8** is observed (the ends of which are marked by arrows 3/5 and 4/6 in Figure 1b/d), where the rigid rods adopt an angle of γ (c', c'') = $(96 \pm 2)°$.

These results motivated us to investigate **1**, its precursor **8** (containing three phenylene–ethynylene rods of two different lengths, connected by two azobenzene units), and **6b** (containing two "short" phenylene–ethynylene rods con-

nected to one azobenzene unit) by means of UV/vis spectroscopy (see SI). When a solution of 6×10^{-6} M of **1** in toluene was prepared and allowed to stand for 2 h, the UV/vis spectrum showed two maxima at 319 and 421 nm. Irradiation with a light-emitting diode with 410 nm maximum wavelength and a FWHM of 20 nm (see SI) did not lead to any discernible spectral change (see SI). After preparing solutions of **8** and **6b** under identical conditions, absorption maxima at 311, 319 and 416 nm (**8**) as well as 310, 319, and 399 nm (**6b**) were observed. An irradiation at 410 nm for 5 s (or 310 nm for 60 s, **8** and **6b**) led to photostationary states with a minor reduction in absorbance in the spectral range of 300 to 360 nm. Allowing each of the solutions to stand for 5 h in the dark at rt led to a slow increase in absorbance in this region. Azobenzene[21] shows dramatic changes in intensities, and π-extended pyrene derivatives with four azobenzene-ethynyl groups[28] still show significant variations in spectral intensities after irradiation (also for a UV-light-induced back reaction). We attribute the minor intensity changes in **8** and **6b** to the fact that their spectra (particularly at $\lambda > 350$ nm) are determined predominantly by the absorption of the phenylene–ethynylene chromophores (cf. extinction coefficients in Figure S11). The spectrum of **1** does not show any changes after irradiation. This fact is consistent with its ^{1}H NMR spectrum, which does not contain any hint for the presence of the *cis*/*cis* isomer (Figure S1).

We then investigated macrocycle precursor **8** and the half-ring **6b** by 1D and 2D thin-layer chromatography (TLC, see SI). Nominally, we would expect *trans*/*trans*-**8**, *trans*/*cis*-**8**, and *cis*/*cis*-**8** as well as *trans*-**6b** and *cis*-**6b**, and each set of compounds should have different R_f values. Handling the compounds and performing the TLC experiments (using Cy : DCM 1 : 2) in complete darkness led to single peaks for both species (R_f (**8**): 0.33; R_f (**6b**): 0.46). We conclude that these solutions consist of *trans*/*trans*-**8** and *trans*-**6b**, respectively. Exposing **8** (and **6b**) to daylight (either before and during its application to the TLC plate, or after dissolving and depositing the compound and performing a first TLC run in darkness) or 410 nm (while otherwise handling the compound in darkness) led to additional spots (with R_f (**8**) = 0.21 and R_f (**6b**) = 0.24). Unexpectedly, a third spot, indicative of a third switching state, was not observed for **8**. This absence might be explained by either identical R_f values or concerted *trans*–*cis*-isomerization of both azobenzene units after photon absorption. This observation is consistent with the STM experiment described before where *trans*/*trans* and *cis*/*cis* isomers were observed yet. Exposure of **6b** during the TLC run led to smeared peaks, indicative of *trans*–*cis* (and *cis*–*trans*) isomerization on the TLC timescale.

Ensemble measurements to investigate the photophysical properties of **1** were performed in toluene solution. Figure 2a shows the normalized absorption ($\lambda_{Max}^{Abs} \approx 420$ nm) and photoluminescence (PL) spectra ($\lambda_{Max}^{PL} \approx 470$ nm) under excitation at 410 nm (green curves). In order to compare the results with our previously synthesized structures, we also show the spectra of the rigid clamp reference **2** (Scheme 1) with a chromophore spacing of approx. 0.7 nm (black).[12] Both the absorption and emission spectra of compound **1** are blue-shifted compared to this earlier bichromophoric structure. The blue-shift in the absorption of **1** presumably originates from the inductive effects of the azobenzene clamps. Figure 2b shows the PL decay of **1** (green curve) in toluene solution, measured under pulsed laser excitation using time-correlated single-photon counting (TCSPC) together with the instrument response function (IRF) of the TCSPC system used (gray). By reconvolution of the signal with the IRF, we fit the data using a biexponential function (red) with decay times of $\tau_1 = 25$ ps and $\tau_2 = 648$ ps, where the latter value is determined by a tail fit of the decay. This biexponential decay profile of **1** is in stark contrast to that of the rigid clamp reference **2**, where a monoexponential decay was observed with a PL lifetime of 660 ps.[12]

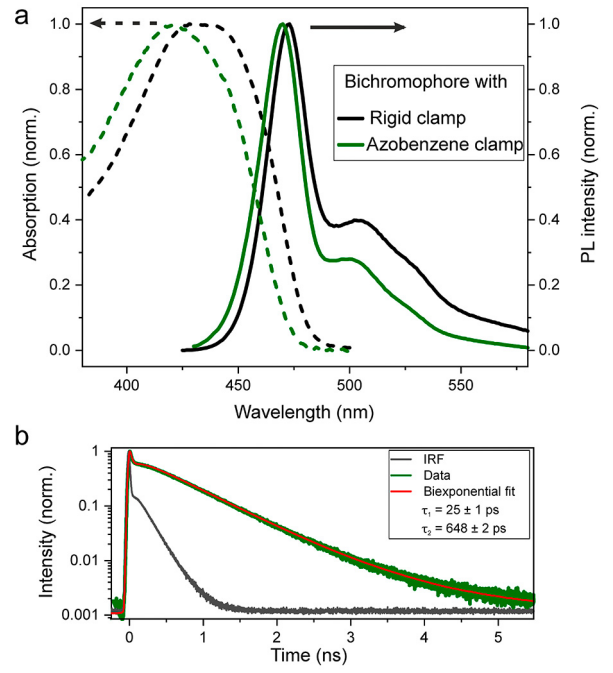

Figure 2 Ensemble spectroscopy in toluene solution: (a) normalized absorption (dotted lines) and emission (solid lines) spectra of compound **1** (green) and the bichromophoric system **2** with rigid clamping units and a 0.7 nm interchromophoric spacing (black). (b) PL intensity decay transient of **1** (green) together with the instrument response function (IRF; gray) of the TCSPC system used. The biexponential fit (red) is achieved by reconvolution of the signal with the IRF and by performing a tail fit of the signal to reveal the dominant time constants $\tau_1 = (25 \pm 1)$ ps and $\tau_2 = (648 \pm 2)$ ps.

As we showed in earlier work, the dependence of the PL spectra and PL lifetime on the interchromophore distance can be described in the framework of H-type electronic cou-

pling of molecular aggregates.[13,29] As the chromophore separation decreases, the PL spectrum is shifted to lower photon energies and the oscillator strength of the radiative transition decreases. The comparison with the 0.7 nm-spaced rigid clamp reference **2** in Figure 2 indicates a slightly increased chromophore spacing of the azobenzene bichromophore **1**, and hence the PL spectrum of **1** is blue-shifted and the PL lifetime is slightly lowered to $\tau_2 = 648$ ps with respect to **2**. This observation agrees with the STM measurements shown in Figure S4, which suggest a chromophore separation in **1** of between 0.8 and 1.6 nm. In order to identify the origin of the unexpectedly fast PL lifetime component of **1**, we measured the PL quantum yield (PLQY) using the commercial dye ATTO 390 as a reference standard and found a value of (4 ± 0.4)%. This value is strongly reduced compared to the previously reported rigid clamp bichromophoric system, where a value of > 60% was measured.[10] Therefore, we conclude that the fast PL decay component of $\tau_1 = 25$ ps follows a fast nonradiative recombination pathway, which is only present in compound **1** but not in the rigidly clamped reference **2**.

This conclusion raises the question of whether the multiexponential fluorescence decay in solution is related to the occurrence of multiple subpopulations or conformations of the molecules, or whether these dynamics can also be observed on the level of single isolated molecules. Single-molecule spectroscopy offers direct access to answering this question. By strongly diluting the analyte into a 2 wt% PMMA–toluene solution, we can immobilize single molecules by spin coating this mixture onto microscope glass cover slips to form a PMMA film of approx. 50 nm thickness. The concentration of the analyte within the PMMA/toluene solution determines the density of immobilized molecules observed in confocal scan images of the microscope as shown in Figure 3. We adjusted the analyte concentration of both the previously studied rigid clamp reference **2** and of sample **1** prior to spin coating to the very same concentration and show the resulting confocal microscopy scan images in Figure 3. For the same concentration, we find a strongly reduced fluorescence spot density of (0.011 ± 0.004) μm^{-2} for compound **1** compared to the rigid clamp structures **2** with a spot density of (0.176 ± 0.008) μm^{-2}.

Figures 3(c, d) shows example TCSPC traces (black curves) of the rigid and azobenzene bichromophoric clamp structures **2** and **1**, respectively, together with single-exponential tail fits (red lines). The time constants extracted are stated in the figure. Surprisingly, unlike in the ensemble measurements, the average single-molecule PL lifetimes are almost identical for both samples ((0.83 ± 0.17) ns for **1** vs. (0.89 ± 0.2) ns for **2**), even though the lifetimes scatter within each sample. A statistical analysis of this observation is shown in Figure S16 of the SI. The most important observation is that all measured spots of **1** show a single-exponential PL decay without any fast lifetime component, unlike the ensemble measurements in Figure 2. We therefore conclude that two subpopulations must be present within the ensemble of compound **1**. The first group exhibits photophysical properties comparable to the previously reported rigid clamp reference **2**. However, since the density of visible spots is approximately 16 times lower for **1** than for the rigid clamp reference **2**, the results indicate that most single molecules of **1** show strong fluorescence quenching, i.e. nonradiative recombination, leading to the low PL lifetime component τ_1 and the low PLQY in solution. Due to this low brightness, we cannot detect this subpopulation at the single-molecule level. This strong quenching also agrees with the PLQY ratio of the two compounds of approx. 60% to 4% (≈ 15). Since a *trans–cis* switching of the azo moieties in **1** can be excluded, it is conceivable that the azobenzene groups themselves directly influence the nonradiative decay pathways of the chromophores. On the one hand, such quenching could also conceivably be caused by the flexibility and mobility of the clamp pieces, as has already been observed for molecular rotors such as BODIPY dye molecules.[30,31] On the other hand, it is also possible that energy or electron transfer occurs to the azobenzene groups, for which low fluorescence quantum yields have already been reported.[32] A possibility to test whether efficient energy transfer can occur within the clamped bichromophore structure **2** is to measure the fluorescence photon statistics of single molecules as discussed in Figure S16 of the SI. For both compound **1** and the analogous rigid clamp structure **2**, we find nearly perfect single-photon emission, i.e. so-called photon antibunching, in the single-molecule fluorescence. In a multi-

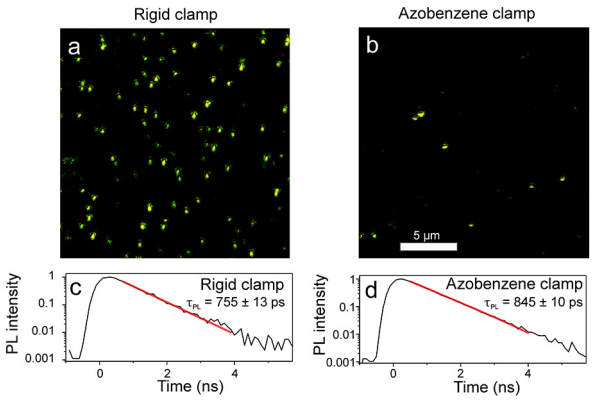

Figure 3 Single molecule spectroscopy: (a) and (b) show confocal scan images with dimensions of (20 × 20) μm^2 of the 0.7 nm rigid clamp structures **2** and azobenzene-clamped bichromophore **1**, respectively. From these images, we extract spot densities of (0.176 ± 0.008) μm^{-2} and (0.011 ± 0.004) μm^{-2}, respectively. (c) and (d) show examples of single-molecule PL decays (black) together with monoexponential fits (red lines).

chromophoric molecule such as **1**, this effect can only occur if multiple excitons, which are present at the same time, can diffuse in space and annihilate via bimolecular recombination pathways, i.e. singlet–singlet annihilation.[32] The nearly perfect single-photon emission of **1** shows that efficient energy transfer indeed takes place between the two chromophores within the molecule. It is also conceivable that, under certain circumstances, a transfer process to the azobenzene clamp units might be possible and thereby quench the excited-state population.

Conclusions

An azo-clamped bichromophoric cyclophane was successfully synthesized by the intramolecular Pd(II) and Cu(I) catalyzed coupling of the corresponding bisacetylenic precursor. While a photoinduced switching of the precursors could indeed be observed, most easily by TLC, the final cyclophane does not show any switching behavior. STM investigations prove the overall structure of the cyclophane and show that its open precursor adopts *trans*/*trans* and also *cis*/*cis* configurations. Photophysical investigations show that most of the fluorescence is quenched, which we attribute to the influence of the azo clamp in the molecule. However, bright molecules show nearly perfect single-photon emission, meaning that efficient energy transfer between the two chromophores takes place within the molecule.

Experimental Section

Reagents and analytics. Reagents were purchased at reagent grade from commercial sources and used without further purification. All air-sensitive reactions were carried out using standard Schlenk techniques under argon. 2-Bromo-5-iodo hydroquinone (**8**) was prepared as described in Ref. [33].[33] [(3-Cyanopropyl) diisopropylsilyl] acetylene (CPD*i*PS-acetylene) and [(3-cyanopropyl dimethylsilyl] acetylene (CPDMS-acetylene) were prepared as described in Ref. [34].[34] Diiodo azobenzene (**2**) was prepared as described in Ref. [35].[35] Reaction solvents (tetrahydrofuran, piperidine, dichloromethane, pyridine, triethylamine, toluene) were dried, distilled, and stored under argon according to standard methods; workup solvents were either used in "p.a." quality or purified by distillation (dichloromethane, cyclohexane). Prior to characterization and further processing, all solids and oils were dried at rt under vacuum. ^{1}H and ^{13}C NMR spectra were recorded on a Bruker Avance I 300 MHz, a Bruker Avance I 400 MHz, a Bruker Avance III HD 500 MHz Prodigy and a Bruker Avance III HD 700 MHz Cryo (300.1, 400.1, 500.1 and 700.1 MHz for ^{1}H and 75.5, 100.6, 125.8 and 176.0 MHz for ^{13}C). Chemical shifts are given in parts per million (ppm) referenced to residual ^{1}H or ^{13}C signals in deuterated solvents. All NMR spectra were recorded at rt unless otherwise described. Mass spectra were measured on a Finnigan ThermoQuest MAT 95 XL (EI-MS), a Sektorfeldgerät MAT 90 (EI-MS), a Bruker Daltonics micrOTOF-Q (ESI-MS, APCI), a Bruker Daltonics autoflex TOF/TOF (MALDI-MS; matrix material: DCTB, no salts added) and an ultrafleXtreme TOF/TOF of the Bruker Daltonik company (MALDI-MS; matrix material: DCTB, no salts added). TLC was conducted on silica gel-coated aluminium plates (Macherey-Nagel, Alugram SIL G/UV254, 0.25 mm coating with fluorescence indicator). Silica gel Kieselgel 60 (Merck, 0.040 – 0.063 mm) was used as the stationary phase for column chromatography. UV/vis absorption spectra were recorded on a Perkin Elmer Lambda 18 and fluorescence emission spectra on a Perkin Elmer LS-50B spectrophotometer using 10 mm quartz cuvettes.

Gel permeation chromatography (GPC). GPC was performed in THF (HPLC grade, stabilized with 2.5 ppm BHT) at rt. GPC analyses were run on an Agilent Technologies system at a flow rate of 1 mL/min using an IsoPump (G1310 A), a diode array UV detector (G1315B) and PSS columns (Polymer Standards Service; Mainz, Germany; 10^2, 10^3, 10^5 and 10^6 Å, 5 µ, 8 × 300 mm). All molecular weights were determined vs. PS calibration (PS standards from PSS, Mainz, Germany).

For the preparative separation, a Shimadzu rec GPC system, equipped with an LC-20 AD pump, an SPD-20 A UV detector and a set of three preparative columns from PSS (either SDV 10^3 Å, 5 µ, 20 × 300 mm or SDV preparative linear S, 5 µ, 20 × 300 mm) with precolumn (SDV, 5 µ, 20 × 50 mm) was employed. The system operated at a flow rate of 5 mL/min, THF, 35 °C.

Scanning tunneling microscopy (STM). STM was performed under ambient conditions (rt) at the solution/solid interface, using TCB as the solvent and HOPG as the substrate. In a typical experiment, 0.2 µL of a 5×10^{-6} M to 1×10^{-5} M solution of the compound of interest was dropped onto a freshly cleaved HOPG substrate at elevated temperature (80 °C), kept at this temperature for 20 s, and allowed to cool to rt before the STM measurements were performed with the tip immersed into the solution. Bias voltages between −0.8 and −1.2 V and tunneling current set points in the range of 26 – 117 pA were applied to image the supramolecular adlayers shown here. The experimental setup consists of an Agilent 5500 scanning probe microscope that is placed on a Halcyonics actively isolated microscopy workstation. It is acoustically shielded with a home-built box. Scissors cut Pt/Ir (80/20) tips were used and further modified after approach by applying short-voltage pulses until the desired resolution was achieved. HOPG was obtained from TipsNano (via Anfatec) in ZYB-SS and DS quality. All STM images (unless otherwise noted) were calibrated by subsequent immediate acquisition of an additional image at a reduced bias voltage, therefore the atomic lattice of the HOPG surface is observed, which is used as a calibration grid.

Data processing, also for image calibration, was performed using the SPIP 5 (Image Metrology) software package.

(Supra-)molecular modelling. (Supra-)molecular modelling was performed using Wavefunction Spartan '18. Equilibrium geometries shown in Figure S4 were obtained using molecular mechanics (based on the Merck molecular force field) and a graphene monolayer with fixed atom positions as the interaction partner. Equilibrium geometries shown in Figure S7(b – g) were obtained with the same method, however using three different starting geometries. These were manually created to match the shapes observed in the STM image shown in Figure S7a (arrows 1 – 6). Moreover, dihedral angles of the azobenzene units were frozen to obtain the *trans* or *cis* isomers. The molecular models shown in Figure 1c were obtained from the backbone structure shown in Figure S4(a, b) and subsequently added all-*trans*-configured alkoxy side chains oriented along the HOPG main axis directions observed in the STM image, and these molecules were used to create the supramolecular model. The supramolecular model shown in Figure 1d was obtained in a similar procedure to match the structures observed in the STM image shown in Figure 1b.

Optical spectroscopy. UV/vis absorption spectra shown in Figures S9–S11 were recorded on a Perkin Elmer Lambda 18 spectrometer using 10 mm quartz cuvettes.

Ensemble absorption and PL spectra shown in Figure 2 were recorded by dissolving the analyte in toluene solution and filling this into a 10 mm quartz cuvette (Hellma Analytics, Quartz SUPRASIL). The data were recorded using a Perkin Elmer spectrometer (Lambda 650) for absorption and a Horiba Jobin Yvon Fluoromax 4 for PL. Spectra were background-corrected and normalized.

The PL decay of **1** in toluene solution was measured on an inverted confocal microscope as described elsewhere (Figure S6). A frequency-doubled Ti : sapphire oscillator (Spectra Physics Mai Tai BB) operating at 440 nm and 80 MHz repetition frequency was used for excitation. Using a single-photon counting module (Picoquant-MPD-050-CTB), we recorded the signal over a time period of 5 minutes. The extracted PL lifetimes shown in Figure 2b were confirmed by additional measurements using a picosecond streak-camera system (data not shown).

Single-molecule measurements were performed under excitation at a wavelength of 440 nm with a power density of approx. 750 Wcm^{-2} using two single-photon detectors (Picoquant-π-SPAD-20) in a Hanbury Brown and Twiss detection geometry.

Synthetic procedures

Synthesis of 5: Under an Ar atmosphere, **3** (36.0 mg, 71 µmol)[35], **4** (200.0 mg, 0.18 mmol), $Pd(PPh_3)_4$ (9.5 mg, 0.008 mmol), and CuI (1.0 mg, 0.004 mmol) in piperidine (15 mL) and THF (5 mL) were stirred at rt for 6 d. Water and CH_2Cl_2 were added, the aqueous phase was extracted with CH_2Cl_2, and the organic phase was washed with aqueous HCl (2 M), water and brine and dried over $MgSO_4$. After evaporation of the solvent, column chromatographic purification (Cy : DCM = 1 : 1 → 2 : 3; R_f = 0.53 (2 : 3)) gave **5** as a yellow film (139.8 mg, 58 µmol, 71 %).
Formula: $C_{156}H_{216}N_4O_{12}Si_2$, molar mass: 2395.63 g/mol.
^{1}H NMR (500 MHz, $CDCl_3$, rt) δ [ppm]: 8.10 (t, $^4J_{HH}$ = 1.8 Hz, 2 H), 7.91 (ddd, $^3J_{HH}$ = 8.0 Hz, $^4J_{HH}$ = 2.0 Hz, $^4J_{HH}$ = 1.2 Hz, 2 H), 7.65 (dt, $^3J_{HH}$ = 7.7 Hz, $^4J_{HH}$ = 1.3 Hz, 2 H), 7.52 (t, $^3J_{HH}$ = 7.8 Hz, 2 H), 7.05 (s, 2 H), 7.04 (s, 2 H), 7.02 (s, 2 H), 7.01 (s, 2 H), 6.96 (s, 2 H), 6.93 (s, 2 H), 4.08 – 4.00 (m, 20 H), 3.96 (t, $^3J_{HH}$ = 6.4 Hz, 4 H), 2.44 (t, $^3J_{HH}$ = 7.0 Hz, 4 H), 1.94 – 1.81 (m, 28 H), 1.61 – 1.46 (m, 24 H), 1.43 – 1.24 (m, 48 H), 1.15 – 1.06 (m, 28 H), 0.94 – 0.82 (m, 40 H).
^{13}C NMR (126 MHz, $CDCl_3$, rt) δ [ppm]: 154.5, 153.9, 153.7, 153.4, 152.5, 134.2, 129.3, 125.9, 124.7, 123.2, 119.9, 118.0, 117.4, 117.4, 117.3, 116.6, 115.0, 114.8, 114.5, 114.4, 113.8, 113.4, 104.1, 95.3, 94.2, 91.8, 91.8, 91.7, 91.6, 87.1, 70.0, 69.9, 69.9, 69.8, 69.3, 31.8, 31.8, 29.9, 29.6, 29.5, 29.5, 29.5, 27.1, 26.0, 26.0, 25.9, 25.8, 25.8, 22.8, 22.8, 21.5, 20.9, 18.4, 18.2, 14.2, 14.2, 12.0, 9.8, 1.2.
MS (MALDI-TOF, DCTB) *m*/*z*: 2393.6 $[M]^+$, 2643.7 $[M + DCTB]^+$.
Calculated exact mass: 2393.60 g/mol.

Synthesis of 6a and 6b: Under an Ar atmosphere, TBAF (1 M in THF, 0.1 mL, 0.1 mmol) was added to **5** (130.0 mg, 54 µmol) in THF (6 mL) and water (0.24 mL). After 1 h, 1.5 h, and 2.5 h, additional portions of TBAF (each 0.1 mL, 0.1 mmol) were added. After a total reaction time of 5 h, water and CH_2Cl_2 were added, the aqueous phase was extracted with CH_2Cl_2, and the organic phase was washed with water and brine and dried over $MgSO_4$. After evaporation of the solvent, column chromatographic purification (Cy : DCM = 2 : 3 → 1 : 2, R_f = 0.64 (1 : 2)) and additional purification by rec GPC gave **6a** as a yellow film (38.5 mg, 0.02 mmol, 32 %). In addition, **6b** was also obtained as a yellow film (32.5 mg, 16.0 µmol, 29 %) (Cy : DCM = 2 : 3 → 1 : 2, R_f = 0.70 (1 : 2)).
6a: Formula: $C_{146}H_{197}N_3O_{12}Si$, molar mass: 2214.28 g/mol.
^{1}H NMR (500 MHz, $CDCl_3$, rt) δ [ppm]: 8.10 (t, $^4J_{HH}$ = 2.0 Hz, 2 H), 7.92 – 7.89 (m, 2 H), 7.65 (d, $^3J_{HH}$ = 7.6 Hz, 2 H), 7.52 (t, $^3J_{HH}$ = 7.8 Hz, 2 H), 7.07 – 6.91 (m, 12 H), 4.10 – 3.93 (m, 24 H), 3.34 (s, 1 H), 2.44 (t, $^3J_{HH}$ = 7.0 Hz, 2 H), 1.94 – 1.75 (m, 26 H), 1.62 – 1.42 (m, 24 H), 1.42 – 1.28 (m, 48 H), 1.16 – 1.04 (m, 14 H), 0.94 – 0.81 (m, 38 H).
^{13}C NMR (126 MHz, $CDCl_3$, rt) δ [ppm]: 154.5, 154.3, 153.9, 153.7, 153.5, 153.4, 152.5, 134.2, 129.3, 125.9, 124.7, 123.2, 119.9, 118.1, 117.9, 117.4, 117.3, 117.2, 116.6, 114.8, 114.4, 113.8, 113.4, 112.7, 104.1, 95.3, 94.2, 91.7, 91.7, 91.4, 87.1, 82.4, 80.2, 70.0, 69.9, 69.8, 69.8, 69.8, 69.7, 69.3, 31.8, 31.8, 31.8, 31.7, 29.9, 29.5, 29.5, 29.5, 29.4, 29.4, 29.4, 29.3, 26.0,

25.9, 25.9, 25.8, 25.8, 25.8, 25.8, 22.8, 22.8, 22.7, 21.5, 20.9, 18.4, 18.2, 14.2, 14.2, 14.2, 12.0, 9.8.
MS (MALDI-TOF, DCTB) *m/z*: 2212.4 $[M]^+$, 2462.5 $[M + DCTB]^+$.
Calculated exact mass: 2212.47 g/mol.

6b: Formula: $C_{136}H_{178}N_2O_{12}$, molar mass: 2032.92 g/mol.
^{1}H NMR (500 MHz, $CDCl_3$, rt) δ [ppm]: 8.10 (t, $^4J_{HH}$ = 1.9 Hz, 2 H), 7.91 (dt, $^3J_{HH}$ = 8.0 Hz, $^4J_{HH}$ = 1.6 Hz, 2 H), 7.65 (dt, $^3J_{HH}$ = 7.7 Hz, $^4J_{HH}$ = 1.5 Hz, 2 H), 7.52 (t, $^3J_{HH}$ = 7.8 Hz, 2 H), 7.05 (s, 1 H), 7.04 (s, 1 H), 7.02 (s, 1 H), 7.01 (s, 1 H), 7.00 (s, 1 H), 6.98 (s, 1 H), 4.09 – 3.98 (m, 24 H), 3.34 (s, 2 H), 1.91 – 1.79 (m, 24 H), 1.61 – 1.46 (m, 24 H), 1.43 – 1.30 (m, 24 H), 1.30 – 1.17 (m, 24 H), 0.94 – 0.82 (m, 36 H).
^{13}C NMR (126 MHz, $CDCl_3$, rt) δ [ppm]: 154.3, 153.9, 153.7, 153.7, 153.5, 152.5, 134.2, 129.3, 125.9, 124.7, 123.2, 118.1, 117.4, 117.3, 117.2, 115.1, 114.8, 114.5, 114.4, 113.8, 112.7, 94.2, 91.8, 91.7, 91.7, 91.4, 87.1, 82.4, 80.2, 69.9, 69.9, 69.8, 69.8, 69.8, 32.1, 31.8, 31.8, 31.8, 31.7, 29.9, 29.5, 29.5, 29.5, 29.4, 29.4, 29.3, 26.0, 25.8, 25.8, 25.8, 25.8, 22.8, 22.8, 22.8, 22.7, 14.3, 14.2, 14.2, 14.2.
MS (MALDI-TOF, DCTB) *m/z*: 2031.3 $[M]^+$, 2281.4 $[M + DCTB]^+$.
Calculated exact mass: 2031.34 g/mol.

Synthesis of 7: Under an Ar atmosphere, **6a** (78.5 mg, 36 µmol), $Pd(PPh_3)_2Cl_2$ (7.5 mg, 0.01 mmol), CuI (5.1 mg, 0.03 mmol), and I_2 (16.2 mg, 0.06 mmol) in $HN(iPr)_2$ (5 mL) and THF (7 mL) were stirred at rt for 16 h. Water and CH_2Cl_2 were added, the aqueous phase was extracted with CH_2Cl_2, and the organic phase was washed with aqueous HCl (1 M), water, and brine and dried over $MgSO_4$. After evaporation of the solvent, column chromatographic purification (Cy : DCM = 2 : 3 → 1 : 2, R_f = 0.45 (1 : 2)) and additional purification by rec GPC gave **7** as an orange film (37.7 mg, 8.5 µmol, 48 %).
Formula: $C_{292}H_{392}N_6O_{24}Si_2$, molar mass: 4426.54 g/mol.
^{1}H NMR (500 MHz, $CDCl_3$, rt) δ [ppm]: 8.10 (s, 4 H), 7.91 (d, $^3J_{HH}$ = 8.0 Hz, 4 H), 7.65 (d, $^3J_{HH}$ = 7.6 Hz, 4 H), 7.52 (t, $^3J_{HH}$ = 7.8 Hz, 4 H), 7.06 – 6.92 (m, 24 H), 4.09 – 3.94 (m, 48 H), 2.43 (t, $^3J_{HH}$ = 6.9 Hz, 4 H), 1.92 – 1.76 (m, 52 H), 1.62 – 1.46 (m, 48 H), 1.41 – 1.28 (m, 96 H), 1.16 – 1.07 (m, 28 H), 0.95 – 0.80 (m, 76 H).
^{13}C NMR (126 MHz, $CDCl_3$, rt) δ [ppm]: 155.2, 154.5, 153.9, 153.7, 153.7, 153.5, 153.4, 152.6, 134.2, 129.3, 125.9, 125.7, 124.7, 123.2, 120.0, 118.0, 118.0, 117.4, 117.3, 117.3, 116.6, 115.6, 115.0, 114.8, 114.5, 114.4, 113.8, 113.4, 95.3, 94.2, 91.8, 91.8, 87.1, 70.0, 69.9, 69.9, 69.8, 69.3, 32.8, 32.1, 31.8, 31.8, 31.8, 31.7, 30.5, 29.9, 29.5, 29.5, 29.5, 29.4, 29.4, 29.3, 26.0, 26.0, 26.0, 25.8, 25.8, 25.8, 22.8, 22.8, 21.5, 20.9, 18.4, 18.2, 14.2, 12.0, 9.8, 1.2.
MS (MALDI-TOF, DCTB) *m/z*: 4422.9 $[M]^+$, 4673.1 $[M + DCTB]^+$, 4923.2 $[M + 2DCTB]^+$.
Calculated exact mass: 4422.92 g/mol.

Synthesis of 8: Under an Ar atmosphere, TBAF (1 M in THF, 0.07 mL, 0.07 mmol) was added to **7** (50.0 mg, 11 µmol) in THF (7 mL) and stirred at rt for 12 h. Water and CH_2Cl_2 were added, the aqueous phase was extracted with CH_2Cl_2, and the organic phase was washed with water and brine and dried over $MgSO_4$. After evaporation of the solvent, column chromatographic purification (Cy : DCM = 1 : 1, R_f = 0.58) and additional purification by rec GPC gave **8** as a yellow film (37 mg, 9 µmol, 81 %).
Formula: $C_{272}H_{354}N_4O_{24}$, molar mass: 4063.83 g/mol.
^{1}H NMR (500 MHz, $CDCl_3$, rt) δ [ppm]: 8.11 – 8.09 (m, 4 H), 7.94 – 7.88 (m, 4 H), 7.67 – 7.64 (m, 4 H), 7.52 (t, $^3J_{HH}$ = 7.8 Hz, 4 H), 7.06 – 6.97 (m, 24 H), 4.09 – 3.98 (m, 48 H), 3.34 (s, 2H), 1.92 – 1.77 (m, 48 H), 1.61 – 1.46 (m, 48 H), 1.42 – 1.29 (m, 96 H), 0.96 – 0.85 (m, 72 H).
^{13}C NMR (126 MHz, $CDCl_3$, rt) δ [ppm]: 155.1, 154.3, 153.9, 153.7, 153.7, 153.7, 153.5, 153.5, 153.3, 152.5, 134.2, 130.9, 129.3, 128.8, 125.9, 124.7, 124.3, 123.2, 118.1, 118.0, 117.4, 117.3, 117.2, 117.2, 115.6, 115.1, 114.8, 114.6, 114.5, 114.4, 114.3, 113.8, 112.7, 94.2, 92.4, 91.8, 91.7, 91.7, 91.5, 91.4, 87.1, 82.4, 80.2, 79.8, 79.5, 69.9, 69.9, 69.8, 69.8, 69.8, 69.7, 31.8, 31.8, 31.8, 31.7, 31.7, 29.5, 29.5, 29.4, 29.4, 29.4, 29.3, 29.3, 26.0, 25.8, 25.8, 25.8, 25.8, 25.8, 22.8, 22.8, 22.8, 22.7, 14.2, 14.2, 1.2.
MS (MALDI-TOF, DCTB) *m/z*: 4060.7 $[M]^+$, 4310.8 $[M + DCTB]^+$, 4561.0 $[M + 2DCTB]^+$.
Calculated exact mass: 4060.66 g/mol.

Synthesis of 1: Under an Ar atmosphere, **8** (10.0 mg, 2.5 µmol) in THF (20 mL) was purged with Ar for 1 h. By using a syringe pump, this solution was slowly added (72 h) to $Pd(PPh_3)_2Cl_2$ (17.3 mg, 24.6 µmol), CuI (2.3 mg, 12.3 µmol), and I_2 (3.5 mg, 13.8 µmol) in THF (20 mL) and $HN(iPr)_2$ (15 mL) at 50 °C and then additionally stirred for 72 h. After cooling to rt, water and CH_2Cl_2 were added, the aqueous phase was extracted with CH_2Cl_2, and the organic phase was washed with water and brine and dried over $MgSO_4$. After evaporation of the solvent, the crude product was dissolved in CH_2Cl_2, filtered through a plug of silica and purified by rec GPC to give **1** as a yellow film (5 – 6 mg, 1.23 – 1.48 µmol, 50 – 60 %; variable yields of different reactions).
Formula: $C_{272}H_{352}N_4O_{24}$, molar mass: 4061.81 g/mol.
^{1}H NMR (700 MHz, $CDCl_3$, rt) δ [ppm]: 8.18 (d, $^4J_{HH}$ = 1.9 Hz, 4 H), 7.94 (dt, $^3J_{HH}$ = 8.1 Hz, $^4J_{HH}$ = 1.4 Hz, 4 H), 7.63 (dt, $^3J_{HH}$ = 7.5 Hz, $^4J_{HH}$ = 1.3 Hz, 4 H), 7.52 (t, $^3J_{HH}$ = 7.7 Hz, 4 H), 7.05 (s, 4 H), 7.04 (s, 4 H), 7.02 (s, 4 H), 7.01 (s, 4 H), 6.99 (s, 4 H), 6.99 (s, 4 H), 4.08 – 3.96 (m, 48 H), 1.89 – 1.75 (m, 48 H), 1.59 – 1.46 (m, 48 H), 1.44 – 1.26 (m, 96 H), 0.94 – 0.80 (m, 72 H).
^{13}C NMR (176 MHz, $CDCl_3$, rt) δ [ppm]: 155.1, 153.9, 153.7, 153.7, 153.7, 153.5, 152.3, 129.3, 124.8, 118.0, 117.4, 117.3, 117.3, 115.6, 114.8, 114.6, 114.4, 113.9, 112.7, 94.2, 92.5, 92.2, 91.6, 79.6, 69.9, 69.9, 69.9, 69.8, 45.4, 32.8, 31.8, 31.8,

31.7, 31.7, 31.2, 29.9, 29.5, 29.5, 29.4, 29.4, 29.4, 29.3, 26.7, 25.9, 25.9, 25.8, 25.8, 25.8, 25.8, 22.8, 22.8, 22.8, 22.7, 14.2, 14.2, 14.1, 14.1, 1.2.
MS (MALDI-TOF, DCTB) *m/z*: 4058.7 $[M]^+$, 4308.8 $[M + DCTB]^+$.
Calculated exact mass: 4058.64 g/mol.

Funding Information

The authors thank the Deutsche Forschungsgemeinschaft for funding through collaborative grant no. 455731873, and RTG-2591 "TIDE-Template-designed Organic Electronics."

Supporting Information

Supporting Information for this article is available online at https://doi.org/10.1055/a-1941-7757.

Conflict of Interest

The authors declare no conflict of interest.

References

(1) Müllen, K.; Scherf, U. *Organic Light-Emitting Devices: Synthesis, Properties and Applications*. Wiley VCH: Weinheim, **2006**.
(2) Klauk, H. *Organic Electronics: Materials, Manufacturing and Applications/Organic Electronics II: More Materials and Applications*. Wiley-VCH: Weinheim, **2006**/**2012**.
(3) Cicoira, F.; Santato, C. *Organic Electronics: Emerging Concepts and Technologies*. Wiley-VCH: Weinheim, **2013**.
(4) Köhler, A.; Bässler, H. *Electronic Processes in Organic Semiconductors: An Introduction*. Wiley-VCH: Weinheim, **2015**.
(5) Schwartz, B. J. *Nat. Mater.* **2008**, *7*, 427.
(6) Scheblykin, I. G. *Nat. Chem.* **2013**, *5*, 903.
(7) (a) Hu, Z. J.; Haws, R. T.; Fei, Z.; Boufflet, P.; Heeney, M.; Rossky, P. J.; Vanden Bout, D. A. *PNAS* **2017**, *114,* 5113. (b) Raithel, D.; Simine, L.; Pickel, S.; Schötz, K.; Panzer, F.; Bederschneider, S.; Schiefer, D.; Lohwasser, R.; Köhler, J.; Thelakkat, M.; Sommer, M.; Köhler, A.; Rossky, P. J.; Hildner, R. *PNAS* **2018**, *115,* 2699.
(8) (a) Noriega, R.; Rivnay, J.; Vandewal, K.; Koch, F. P. V.; Stingelin, N.; Smith, P.; Toney, M. F.; Salleo, A. *Nat. Mater.* **2013**, *12*, 1038. (b) Lupton, J. M. *Adv. Mater.* **2010**, *22,* 1689.
(9) Stangl, T.; Wilhelm, P.; Schmitz, D.; Remmerssen, K.; Henzel, S.; Jester, S.-S.; Höger, S.; Vogelsang, J.; Lupton, J. M. *J. Phys. Chem. Lett.* **2015**, *6*, 1321.
(10) Stangl, T.; Bange, S.; Schmitz, D.; Würsch, D.; Höger, S.; Vogelsang, J.; Lupton, J. M. *J. Am. Chem. Soc.* **2013**, *135*, 78.
(11) Jester, S.-S.; Schmitz, D.; Eberhagen, F.; Höger, S. *Chem. Commun.* **2011**, *47*, 8838.
(12) Liu, S.; Schmitz, D.; Jester, S.-S.; Borys, N. J.; Höger, S.; Lupton, J. M. *J. Phys. Chem. B* **2013**, *117*, 4197.
(13) Allolio, C.; Stangl, T.; Eder, T.; Schmitz, D.; Vogelsang, J.; Höger, S.; Horinek, D.; Lupton; J. M. *J. Phys. Chem. B* **2018**, *122*, 6431.
(14) (a) Giesa, R. *J. Macromol. Sci., Rev. Macromol. Chem. Phys.* **1996**, *C36*, 631. (b) Tour, J. M. *Chem. Rev.* **1996**, *96*, 537. (c) Bunz, U. H. F. *Chem. Rev.* **2000**, *100*, 1605.
(15) (a) Grave, C.; Schlüter, D. *Eur. J. Org. Chem.* **2002**, 3075. (b) Höger, S. *Chem. Eur. J.* **2004**, *10*, 1320. (c) Zhang, W.; Moore, J. S. *Angew. Chem. Int. Ed.* **2006**, *45*, 4416. (d) Iyoda, M.; Yamakawa, J.; Rahman, M. J. *Angew. Chem. Int. Ed.* **2011**, *50*, 10522. (e) Ball, M.; Zhang, B.; Zhong, Y.; Fowler, B.; Xiao, S.; Ng, F.; Steigerwal, M.; Nuckolls, C. *Acc. Chem. Res.* **2019**, *52*, 1068.
(16) (a) Jeschke, G.; Sajid, M.; Schulte, M.; Ramezanian, N.; Volkov, A.; Zimmermann, H.; Godt, A. *J. Am. Chem. Soc.* **2010**, *132*, 10107. (b) Hinderer, F.; May, R.; Jester, S.-S.; Höger, S. *Macromolecules* **2016**, *49*, 1816.
(17) Meißner, S. A.; Eder, T.; Keller, T. J.; Hofmeister, D. A.; Spicher, S.; Jester, S.-S.; Vogelsang, J.; Grimme, S.; Lupton, J. M.; Höger, S. *Nat. Commun.* 2021, 12, 6614.
(18) Müri, M.; Schuermann, K.C.; De Cola, L.; Mayor, M. *Eur. J. Org. Chem.* **2009**, *2009*, 2562.
(19) (a) Mitscherlich, E. *Ann. Phys.* **1834**, *108*, 225. (b) Mitscherlich, E. *Ann. Pharm.* **1834**, *12*, 311.
(20) Glaser, C. *Z. Chem.* **1866**, *9*, 308.
(21) Zollinger, H. *Color Chemistry. Synthesis, Properties, and Applications of Organic Dyes and Pigments*. 3rd ed., Wiley-VCH: Weinheim, **2003**.
(22) Hartley, G. S. *Nature* **1937**, *140*, 281.
(23) (a) Hamo, F.; Djedaini-Pilard, F.; Barbot, F.; Len, C. *Tetrahedron* **2009**, *65*, 10105. (b) Bandara, H. M. D.; Burdette, S. C. *Chem. Soc. Rev.* **2012**, *41*, 1809. (c) Beharry, A. B.; Woolley, G. A. *Chem. Soc. Rev.* **2011**, *40*, 4422. (d) Merino, E.; Ribagorda, M. *Beilstein J. Org. Chem.* **2012**, *8*, 1071. (e) Wagner-Wysiecka, E.; Łukasik, N.; Biernat, J. F.; Luboch, E. *J. Inclusion Phenom. Macrocyclic Chem.* **2018**, *90*, 189. (f) Reuter, R.; Wegner, H. A. *Chem Commun.* **2011**, *47*, 12267.
(24) Lee, S.; Hua, Y.; Flood, A. H. *J. Org. Chem.* **2014**, *79*, 8383.
(25) Jester, S.-S.; Schmitz, D.; Eberhagen, F.; Höger, S. *Chem. Commun.* **2011**, *47*, 8838. For an alternative synthetic approach, see the respective section in the Supporting Information of the present publication.
(26) Reuter, R.; Hostettler, N.; Neuburger, M.; Wegner, H. A. *Eur. J. Org. Chem.* **2009**, *2009*, 5647.
(27) Cojal González, J. D.; Iyoda, M.; Rabe, J. P. *Angew. Chem. Int. Ed.* **2018**, *57*, 17038.
(28) Zeitouny, J.; Belbakra, A.; Llanes-Pallas, A.; Barbieri, A.; Armaroli, N.; Bonifazi, D. *Chem. Commun.* **2011**, *47*, 451.
(29) Eder, T., Vogelsang, J.; Bange, S.; Remmerssen, K.; Schmitz, D.; Jester, S.-S.; Keller, T. J.; Höger, S.; Lupton, J. M. *Angew. Chem. Int. Ed.* **2019**, *58,* 18898.
(30) Liu, X.; Chi, W.; Qiao, Q.; Kokate, S. V.; Cabrera, E.P.; Xu, Z.; Liu, X.; Chang, Y.-T. *ACS Sens.* **2020**, *5,* 731.
(31) Freixas, V. M.; Wilhelm, P.; Nelson, T.; Hinderer, F.; Höger, S.; Tretiak, S.; Lupton, J. M; Fernandez-Alberti, S. *J. Phys. Chem. A.* **2021**, *125,* 8404.
(32) Hofkens, J.; Cotlet, M.; Vosch, T.; Tinnefeld, P.; Weston Kenneth, D.; Ego, C.; Grimsdale, A.; Müllen, K.; Beljonne, D.; Brédas J. L.; Jordens, S.; Schweitzer, G.; Sauer, M.; De Schryver, F. *PNAS* **2003**, *100,* 13146.
(33) Höger, S. *Liebigs Ann. Recl.* **1997**, *1997*, 273.
(34) (a) Höger, S.; Bonrad K. *J. Org. Chem.* **2000**, *65*, 2243. (b) Gaefke, G.; Höger, S. *Synthesis* **2008**, *14*, 2155.
(35) Lee, S.; Hua, Y.; Flood, A. H. *J. Org. Chem.* **2014**, *79*, 8383.